Microwave Photonic Interference Cancellation: RF Analysis, III-V and Silicon Integration, Development of Balanced and Hybrid Architectures

Eric Charles Blow

A Dissertation

Presented to the Faculty

of Princeton University

in Candidacy for the Degree

of Doctor of Philosophy

Recommended for Acceptance

by the Department of

Electrical and Computer Engineering

Advisor: Professor Paul R. Prucnal

January 2024

Contents

List of Tables

List of Figures

Chapter 1

Microwave Photonic Cancellation Theory

Within this chapter, the processing requirements for cancellation systems will be presented as well an introduction to the discrete and integrated photonic implementation. The significant metrics to cancellers: cancellation depth, cancellation bandwidth, and signal-to-noise ratio enhancement will be defined and simulated. Application-specific microwave photonic cancellation architectures are introduced. The source code for the simulations within this chapter is available online: `https://github.com/ericcblow/MWP_RF_Sims`

1.1 Cancellation Processing Requirements

A radio operating within the presence of self-interference (SI) couples strong self-generated RF power which overpowers a weak signal-of-interest. This coupling could occur through a wireless channel of colocated antennas or through an RF circulator. Cancellation is required when the SI signal is in-band with respect to the signal-of-interest (SOI). Under these conditions, traditional filtering is not sufficient for the removal of the SI and doing so yields equal removal of the SOI. Consequently, in-band self-interference requires active signal processing, specifically cancellation, to be successfully removed. As described within the introduction, in-band SI can be generated via advanced duplexed communication, cognitive radio, and adjacent channel leakage [1, 2, 3, 4].

Research on self-interference cancellation via adaptive linear filtering has been ongoing since the 1970s [5]. Within this context, to achieve cancellation of self-interference signals, one

must first obtain a reference interference signal (IRS). The requirement of obtaining an IRS limits the application scope of this approach to self-interference as opposed to blind source separation. Within these systems, the radio's received signal, eqn. 1.1, is a mixture of self-interference and signal-of-interest with an unknown attenuation, α, and time delay τ.

$$Rx(\omega) = \alpha e^{-i\omega\tau}(SOI(\omega) + SI(\omega)) \tag{1.1}$$

The cancellation systems developed within this thesis implement a linear finite impulse response (FIR) filter to match the amplitude, delay, and phase response of the wireless channel [1]. If matched properly, the IRS will be processed by the linear filter and, therefore, will be matched in amplitude, phase, and delay to that of the received SI. Subtracting the matched signals results in the recovery of the SOI. The error of this subtraction is fed back into the linear filter control, resulting in adaptive dynamic cancellation [5]. Audio noise cancellation serves as a signal processing analogy to interference cancellation of wireless radios and is an accessible example of this technique integrated within everyday life.

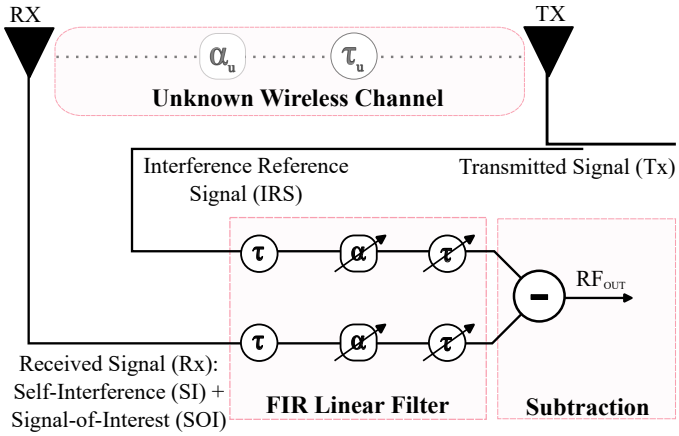

Figure 1.1: Processing requirements for self-interference cancellation.

1.2 Cancellation Metrics and Definitions

There are three metrics which define the cancellation-specific performance of a canceller: cancellation depth (CD), cancellation instantaneous bandwidth C_{IBW}, and cancellation tunability. The cancellation depth, as defined in eqn. 1.2 and shown in Fig. 1.2(left), is the amount of self-interference RF power removed, with cancellation enabled compared to the RF loss of the received path of the canceller without the reference tap active. By defining cancellation depth using this method, the metric is solely a function of active processing and does not account for loss. With respect to a canceller within a fixed state, static linear filter coefficients, the RF bandwidth in which a defined cancellation depth is equal to or greater than is referred to as the cancellation instantaneous bandwidth, eqn. 1.3. The bandwidth in which a single canceller's point of maximum cancellation can be optimized to by adjusting the coefficients of the linear filter is known as the tunability of the canceller, Fig. 1.2 (right). In addition to the cancellation performance metrics, RF performance metrics are of equal importance and are discussed in the following chapter.

$$CD(\omega) = \frac{P_{Rx}(\omega)}{P_{CancelOn}(\omega)} \tag{1.2}$$

$$C_{IBW} = \frac{\int_{BW} P_{Rx}(\omega)}{\int_{BW} P_{CancelOn}(\omega)} \tag{1.3}$$

As shown in [6], the cancellation performance metrics can be equated to the amplitude, phase, and delay mismatch between the received and reference path by modeling the subtraction of the transfer function of both signal paths. In doing so, the model highlights that the cancellation performance is not solely dependent on the matching of transfer functions between the linear filter and the wireless channel, but also fundamentally limited by the matching of the signal path of the canceller and the reference signal path of the cancellation. $X(\omega)$ is the input to the canceller, $Y(\omega)$ is the output of the linear filter, H_{Rx} is the transfer function of the received path, H_{IRS} is the transfer function of the interference reference path of the canceller. In accordance to Fig. 1.1, the output of a general linear filter-based canceller is equal to the difference in transfer function

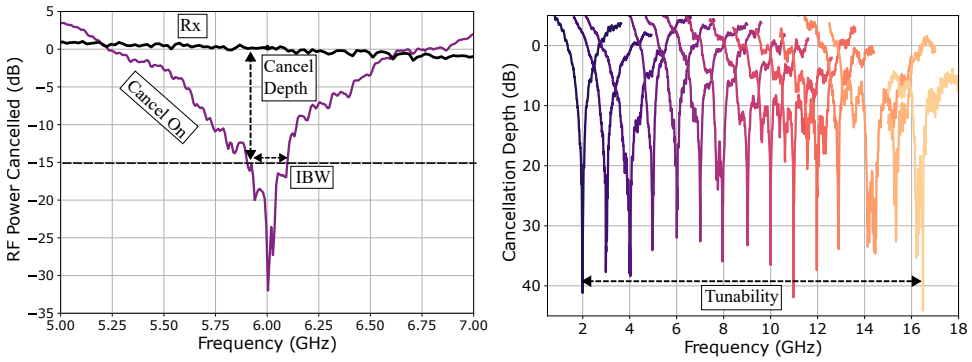

Figure 1.2: Metric Definition for cancellation depth (CD) and cancellation instantaneous bandwidth (IBW) for cancellation system. Black curve is the S21 of the received power, Purple curve is the cancellation transfer function normalized to the S21 of the received path (left). Tunability of cancellation system is demonstrated as one canceller is tuned from 2 GHz to 9 GHz by adjusting coefficients of linear filter (right).

multiplied by the output.

$$Y(\omega) = X(\omega)(H_{Rx} - H_{IRS}) \tag{1.4}$$

The transfer functions of the two paths are equal to the transfer function of the linear FIR filter. In a single-tap architecture, this can be simplified to a weight, α, and a delay, τ. The transfer functions are defined below:

$$\begin{aligned} H_{Rx} &= \alpha_{Rx} e^{-i\omega\tau_{Rx}} \\ H_{IRS} &= \alpha_{IRS} e^{-i\omega\tau_{IRS}} \end{aligned} \tag{1.5}$$

The power transfer function of the canceller can then be defined as the difference in the signal path transfer squared.

$$\left| \frac{Y(\omega)}{X(\omega)} \right|^2 = \left| \alpha_{Rx} e^{-i\omega\tau_{Rx}} - \alpha_{IRS} e^{-i\omega\tau_{IRS}} \right|^2 \tag{1.6}$$

This expression can be further simplified by assuming real values for the linear filter coefficients and can be decomposed to the following:

$$\left|\frac{Y(\omega)}{X(\omega)}\right|^2 = \alpha_{Rx}^2\left(1+\left(\frac{\alpha_{IRS}}{\alpha_{Rx}}\right)^2 - 2\left(\frac{\alpha_{IRS}}{\alpha_{Rx}}\right)cos(\omega(\tau_{IRS}-\tau_{Rx}))\right) \tag{1.7}$$

By defining the amplitude difference of the Rx and IRS path as $\Delta\alpha = \frac{\alpha_{IRS}}{\alpha_{Rx}}$ and the delay difference of the Rx and IRS path as $\Delta\tau = \tau_{IRS} - \tau_{Rx}$ the canceller transfer function can be further simplified.

$$\begin{aligned}\left|\frac{Y(\omega)}{X(\omega)}\right|^2 &= \alpha_{Rx}^2\left(1+(\Delta\alpha)^2 - 2(\Delta\alpha)\,cos(\omega\Delta\tau)\right)\\ CD(\omega) &= 1+(\Delta\alpha)^2 - 2(\Delta\alpha)\,cos(\omega\Delta\tau)\end{aligned} \tag{1.8}$$

These equation implies that with infinite precision and perfect matching, there will be no residual RF interference power. In practice, if the linear filter is precise enough, the RF output will be returned to the noise floor of the canceller. Using eqn. 1.8, the cancellation depth can be simulated as a function of the amplitude and delay difference, shown in Fig. 1.3. Within this figure, the contour lines represent a fixed level of cancellation achievable with a defined required precision of amplitude and delay matching. Horizontal contour lines are phase mismatch limited while vertical lines are amplitude mismatch limited. This is shown in the logarithmic scale with phase mismatch 0.01 dB to 10 dB and amplitude mismatch 0.0001 dB to 1 dB. This simulation is plotted again in Fig. 1.4, with linear scaling of x and y axes to give intuition on the precision required to truly achieve a high level of cancellation. In this figure, the linear scaling of the contour map is projected on $Z = -100dB$. Additionally, the phase and amplitude mismatch is plotted with negative mismatch, implying that Rx is greater power, and positive mismatch, implying that IRS has greater power. This additional information highlights the symmetry of the cancellation cost function.

The bandwidth of cancellation is determined by a difference in frequency-dependent loss and phase shift. If the frequency dependency of the received path and the reference path are perfectly equal, the amplitude and delay mismatch can be corrected with one fixed value, resulting in precision-limited cancellation over the entire operating spectrum. In practice, the two transfer

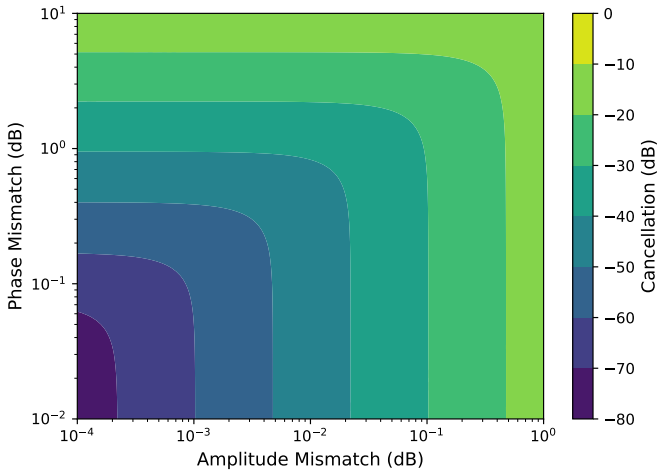

Figure 1.3: Cancellation depth as a function of amplitude and phase mismatch between the two signal paths of a cancellation system. Contour lines highlight required phase and amplitude matching to achieve cancellation depth defined by color bar.

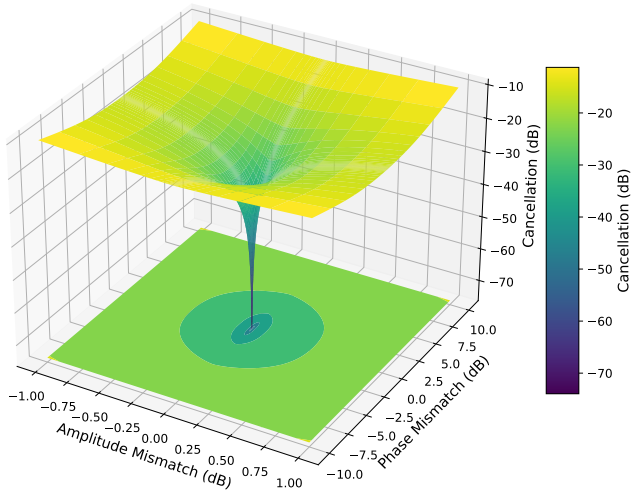

Figure 1.4: Surface plot of cancellation depth as a function of amplitude and phase mismatch between the two signal paths of a cancellation system. The linear scaling of the x-y axis provide intuition on precision required as well as cost function for optimization.

functions will have a difference in frequency-dependent loss and phase and therefore, amplitude and phase mismatch will become dependent on frequency. Since the canceller has fixed linear coefficients, only one frequency point can be optimized for cancellation at a time. Minimizing the change in mismatch as a function of frequency increases the bandwidth of the canceller.

The cancellation-based metrics provides information regarding the amount of RF power being removed by the canceller. This does not fully represent the effect of the canceller on the received signal-of-interest. To more comprehensively evaluate the improvement to the RF chain contributed to the canceller, the signal-to-noise (SNR) enhancement of the SOI should be considered. The SNR enhancement is a function of the amount of interference power removed, cancellation in dB, subtracted by the cancellers SNR degradation due to loss and noise generated. Although introduced and discussed in detail in the next chapter, the SNR degradation due to a black-box system within an RF chain is defined as the noise figure (NF). SNR enhancement is largely missing from the literature and provides a more accurate and comprehensive measurement of the canceller's effectiveness. The SNR enhancement can be defined at a specific frequency or over a bandwidth such as cancellation.

$$SNR_{enhancement}(dB) = Cancellation(dB) - NF_{Canceller}(dB) \tag{1.9}$$

1.3 Microwave Photonic Implementation of Cancellation Requirements

A microwave photonic canceller (MPC) leverages the broadband performance on analog photonic links combined with the tunability of optical linear filtering to create a truly flexible ultra-wide-band cancellation system. An MPC up-converts (modulates) the received and reference high-speed RF signals onto two 193 THz optical carriers. In doing so, the entire wireless spectrum currently utilized becomes narrow-band relative to the carrier [7]. This modulation can be achieved by directly modulating a laser source, interferometric external modulation, or electro-absorption

based modulation. The two modulated optical carriers are passed through an optical linear filter, which matches the self-interference to the interference reference signal.

The linear FIR filter requires amplitude manipulation, phase shifting, and time delaying. Attenuation can be achieved in bulk optics with wideband micro-electromechanical systems (MEMS) variable optical attenuators [8]. This device achieves attenuation by introducing a mode mismatch within a fiber interface. Amplification can be achieved in bulk optics via Erbium-doped Fiber Amplifiers (EDFAs) [9] or solid-state semiconductor variable optical attenuators. Within a silicon integrated photonic platform, attenuation can be achieved with an add-drop silicon microring resonator (MRR) [10] or with a Mach-Zehnder interferometer (MZI) switch [11]. Within an Indium phosphide (InP) integrated platform, tunable amplification and attenuation can be achieved via Multi-Quantum Well (MQW) based semiconductor optical amplifiers (SOAs) [12].

In bulk optical phase shifting and time delaying can be achieved using a MEMS-based device which physically extends the optical path. A continuous implementation could be as simple as a motorized mirror on a mechanical track. Alternatively, the time delay can be discretized, such as within binary switched delays. This system routes optical signals to different paths with varying fixed lengths. Achieving large tunable delay ranges on an integrated platform is a difficult task due to the increase in propagation loss and limited chip real estate. Silicon tunable delays include microring racetrack resonators [13] or simply thermal heating of the fixed section of the waveguide [14]. Discretized delays also include integrated binary switched delay lines which utilize integrated optical switches to route [15]. The linear filter satisfies two matching problems:

1. Matching the attenuation and delay of the wireless channel to the linear filter.

2. Matching the transfer functions of the received path and the reference path.

Following the processing of the linear filter, the two matched signals must be subtracted to cancel the interference. Within a photonic system, subtraction can be achieved coherently or incoherently. Coherent subtraction of the optical signal requires matching the delay and phase of the two optical signals in addition to the modulated carriers, because subtraction occurs within

the optical domain [16]. Incoherent subtraction does not require matching of the optical signals, but only the modulated RF signals. Within an incoherent MPC, the two optical paths have independent photodetectors. If these two photodetectors are isolated, the two photocurrents must be converted to voltage via a resistor or TIA and then subtracted via a Balun. Alternatively, a balanced photodetector can be implemented which electrically configures the photodetectors to generate oppositely flowing photocurrent, resulting in a subtraction of photocurrent at the output. Coherent or incoherent subtraction is a defining difference in microwave photonic cancellers and there are trade-offs in control precision, bandwidth, and cancellation performance [17]. The cancellation systems presented within this thesis will focus on incoherent subtraction of the modulated optical signals. There is parallel promising research on coherent MPCs which can be found in references [18, 19].

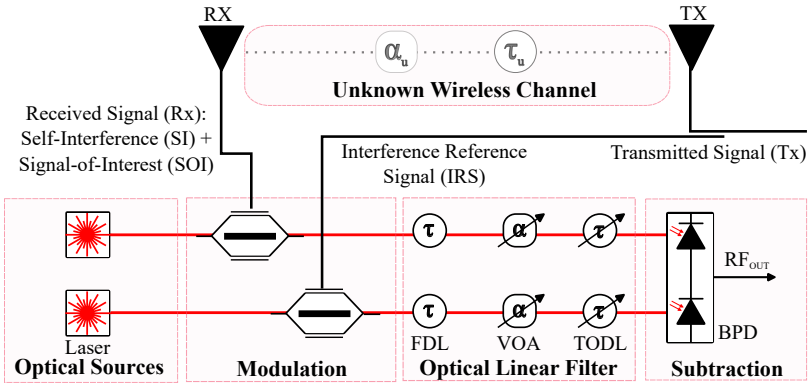

Figure 1.5: Generalized incoherent photonic implementation of microwave photonic canceller. FDL: Fixed Delay Line, VOA: Variable Optical Attenuator, TODL: Tunable Optical Delay Line.

1.4 Application-Specific Architectures

A cancellation system can be scaled in processing complexity from the suppression of one self-interference signal to the suppression of self-interference signals within a multipath and/or multiple-input multiple-output (MIMO) wireless environment. Multiple interference signals can be modeled using a tapped-delay line model, ignoring nonlinear distortion, can be approximated

to have the following transfer function in eqn. 1.10. Therefore, scaling the number of interference signals, N, results in a scaling in the processing complexity by N to achieve the same cancellation depth.

$$\begin{aligned} \left|\frac{Y(\omega)}{X(\omega)}\right|^2 &= \sum_{n=1}^{N} \left|\alpha_{Rx,n} e^{-i\omega\tau_{Rx,n}} - \alpha_{IRS,n} e^{-i\omega\tau_{IRS,n}}\right|^2 \\ CD_{Multipath}(\omega) &= \sum_{n=1}^{N} (1 + (\Delta\alpha_n)^2 - 2\,(\Delta\alpha_n)\, cos(\omega\Delta\tau_n)) \end{aligned} \tag{1.10}$$

1.4.1 Multipath Self-Interference

A multipath wireless environment causes the generation of reflected self-interference signals. The line-of-sight self-interference will still be the higher power signal to cancel but the reflection of the line-of-sight will also couple into the receiver with unknown attenuation, phase, and delay [20]. The FIR optical linear filter must be scaled in the number of taps to compensate for the increased number of interference signals. Note, that the multipath signals are not statistically independent and therefore the IRS can be split and pass through independent linear filter taps. In a MPC multiple optical sources with independent wavelengths can be wavelength division multiplexed (WDM) onto a single optical waveguide and then simultaneously modulated with one interferometric modulator. The modulated WDM signal is then split and processed within the independent taps of the optical linear filter. The processed signals are then recombined onto a single waveguide again before detection. An incident WDM signal onto a photodetector sums the RF signals, which are then subtracted from the received signal. The multipath MPC architecture is shown in Fig. 1.6. Multipath MPCs have been demonstrated in [21, 22, 23, 24]. The resultant cancellation performance increases in complexity by the number of taps, N [25].

1.4.2 Multiple-Input Multiple-Output Self-Interference

Multiple-Input Multiple-Output (MIMO) transceivers are ubiquitous in modern communication networks. If MIMO radios were to operate with cross division or full duplex communication

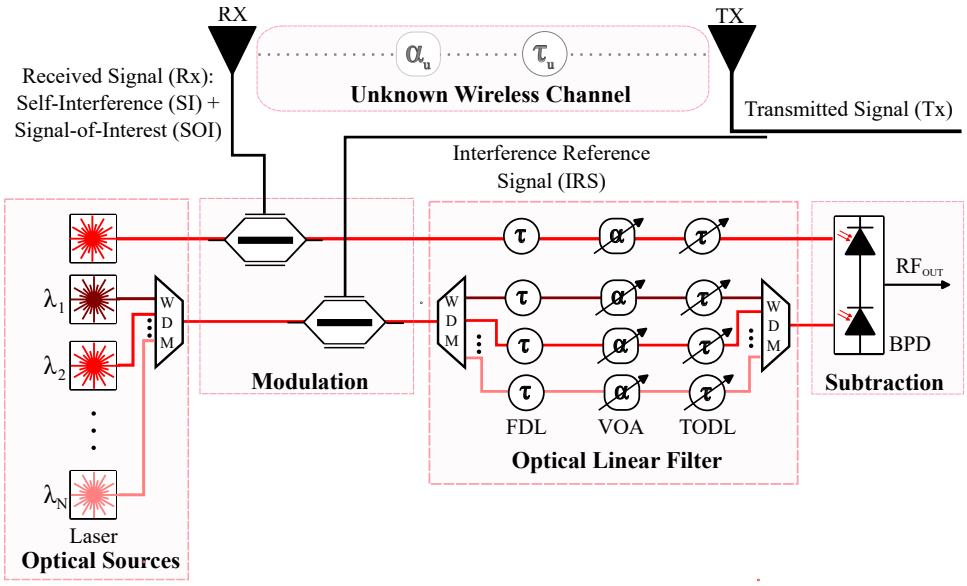

Figure 1.6: Generalized incoherent photonic implementation of microwave photonic canceller with multitap architecture for cancellation of multipath self-interference. FDL: Fixed Delay Line, VOA: Variable Optical Attenuator, TODL: Tunable Optical Delay Line.

standards, multiple independent self-interference signals would be coupled into the receiver [26]. Multiple interference signals can be cancelled similarly to that of a multipath MPC but for each optical tap, independent modulation is required, Fig. 1.7.

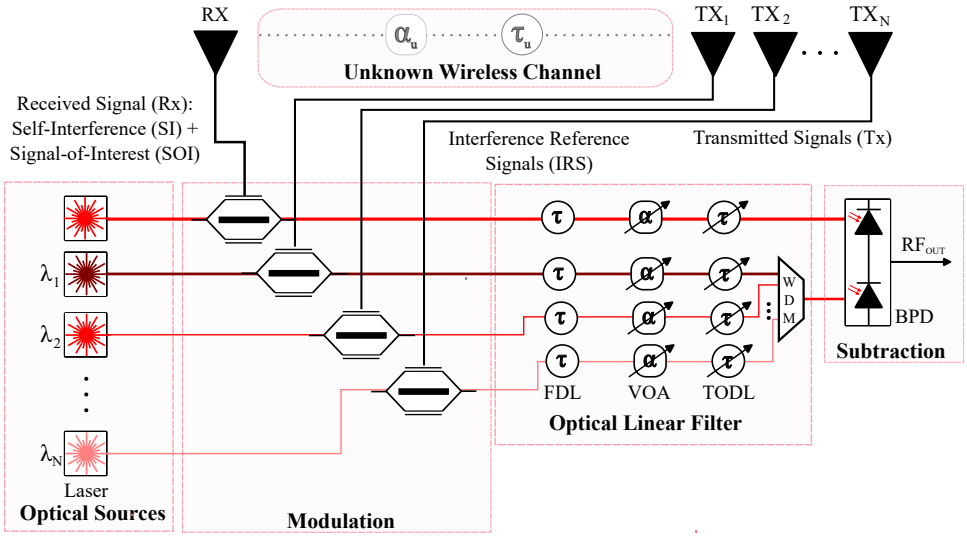

Figure 1.7: Generalized incoherent photonic implementation of microwave photonic canceller with multiple-input multiple-output architecture for cancellation of multiple independent self-interference signals. FDL: Fixed Delay Line, VOA: Variable Optical Attenuator, TODL: Tunable Optical Delay Line.

Bibliography

[1] J. Zhang, F. He, W. Li, Y. Li, Q. Wang, S. Ge, J. Xing, H. Liu, Y. Li, and J. Meng, "Self-interference cancellation: A comprehensive review from circuits and fields perspectives," *Electronics*, vol. 11, no. 2, p. 172, 2022.

[2] S. Hong, J. Brand, J. I. Choi, M. Jain, J. Mehlman, S. Katti, and P. Levis, "Applications of self-interference cancellation in 5g and beyond," *IEEE Communications Magazine*, vol. 52, no. 2, pp. 114–121, 2014.

[3] H. Ji, Y. Kim, K. Muhammad, C. Tarver, M. Tonnemacher, T. Kim, J. Oh, B. Yu, G. Xu, and J. Lee, "Extending 5g tdd coverage with xdd: Cross division duplex," *IEEE Access*, vol. 9, pp. 51380–51392, 2021.

[4] W. Afifi and M. Krunz, "Exploiting self-interference suppression for improved spectrum awareness/efficiency in cognitive radio systems," in *2013 Proceedings IEEE INFOCOM*, pp. 1258–1266, IEEE, 2013.

[5] B. Widrow, J. R. Glover, J. M. McCool, J. Kaunitz, C. S. Williams, R. H. Hearn, J. R. Zeidler, J. E. Dong, and R. C. Goodlin, "Adaptive noise cancelling: Principles and applications," *Proceedings of the IEEE*, vol. 63, no. 12, pp. 1692–1716, 1975.

[6] M. P. Chang, "A microwave photonic interference canceller architectures, systems, and integration," *Princeton University*, 2017.

[7] A. J. Seeds and K. J. Williams, "Microwave photonics," *Journal of lightwave technology*, vol. 24, no. 12, pp. 4628–4641, 2006.

[8] B. Barber, C. Giles, V. Askyuk, R. Ruel, L. Stulz, and D. Bishop, "A fiber connectorized mems variable optical attenuator," *IEEE Photonics Technology Letters*, vol. 10, no. 9, pp. 1262–1264, 1998.

[9] A. Srivastava, Y. Sun, J. Zyskind, and J. Sulhoff, "Edfa transient response to channel loss in wdm transmission system," *IEEE Photonics Technology Letters*, vol. 9, no. 3, pp. 386–388, 1997.

[10] A. N. Tait, A. X. Wu, T. F. De Lima, E. Zhou, B. J. Shastri, M. A. Nahmias, and P. R. Prucnal, "Microring weight banks," *IEEE Journal of Selected Topics in Quantum Electronics*, vol. 22, no. 6, pp. 312–325, 2016.

[11] M. Fokine, L.-E. Nilsson, Å. Claesson, D. Berlemont, L. Kjellberg, L. Krummenacher, and W. Margulis, "Integrated fiber mach–zehnder interferometer for electro-optic switching," *Optics letters*, vol. 27, no. 18, pp. 1643–1645, 2002.

[12] K. Stubkjaer, B. Mikkelsen, T. Djurhuus, N. Storkfelt, C. Jørgensen, K. S. Jepsen, T. N. Nielsen, and U. B. Gliese, "Recent advances in semiconductor optical amplifiers and their applications," in *Fourth International Conference on Indium Phosphide and Related Materials*, pp. 242–245, IEEE, 1992.

[13] J. Cardenas, M. A. Foster, N. Sherwood-Droz, C. B. Poitras, H. L. Lira, B. Zhang, A. L. Gaeta, J. B. Khurgin, P. Morton, and M. Lipson, "Wide-bandwidth continuously tunable optical delay line using silicon microring resonators," *Optics express*, vol. 18, no. 25, pp. 26525–26534, 2010.

[14] W. Bogaerts and L. Chrostowski, "Silicon photonics circuit design: methods, tools and challenges," *Laser & Photonics Reviews*, vol. 12, no. 4, p. 1700237, 2018.

[15] D. Lin, S. Shi, W. Cheng, P. Liu, M. Lu, T. Lin, G. Hu, B. Yun, and Y. Cui, "A high performance silicon nitride optical delay line with good expansibility," *Journal of Lightwave Technology*, vol. 41, no. 1, pp. 209–217, 2022.

[16] R. Paschotta, "Optical heterodyne detection," *RP Photonics Consulting GmbH papers*, 2012.

[17] M. Lu, M. Chang, Y. Deng, and P. R. Prucnal, "Performance comparison of optical interference cancellation system architectures," *Applied optics*, vol. 52, no. 11, pp. 2484–2493, 2013.

[18] Y. Xing, S. Li, X. Xue, and X. Zheng, "Photonic-assisted rf self-interference cancellation based on optical spectrum processing," *Journal of Lightwave Technology*, vol. 40, no. 7, pp. 2015–2022, 2021.

[19] Y. Xing, S. Li, X. Chen, X. Xue, and X. Zheng, "Optical multi-tap rf canceller for in-band full-duplex wireless communication systems," *IEEE Photonics Journal*, vol. 14, no. 5, pp. 1–7, 2022.

[20] J.-H. Lee, J.-w. Choi, J.-H. Jung, S.-C. Kim, and Y.-H. Kim, "Analog cancellation for full-duplex wireless in multipath self-interference channels," *IEICE Transactions on Communications*, vol. 98, no. 4, pp. 646–652, 2015.

[21] J. Chang and P. R. Prucnal, "A novel analog photonic method for broadband multipath interference cancellation," *IEEE Microwave and wireless components Letters*, vol. 23, no. 7, pp. 377–379, 2013.

[22] E. C. Blow, M. P. Chang, and P. R. Prucnal, "Microwave photonic interference canceller: Noise figure reduction via balanced architecture," in *2016 IEEE International Topical Meeting on Microwave Photonics (MWP)*, pp. 157–160, IEEE, 2016.

[23] E. C. Blow, M. P. Chang, and P. R. Prucnal, "Balanced microwave photonic cancellation architecture," *IEEE Microwave Theory and Technique*, 2023 (submitted).

[24] J. J. Sun, M. P. Chang, and P. R. Prucnal, "Demonstration of over-the-air rf self-interference cancellation using an optical system," *IEEE Photonics Technology Letters*, vol. 29, no. 4, pp. 397–400, 2017.

[25] A. F. Molisch, *Wireless communications*. John Wiley & Sons, 2012.

[26] T. L. Marzetta, E. G. Larsson, and H. Yang, *Fundamentals of massive MIMO*. Cambridge University Press, 2016.